

MASS–LUMINOSITY RELATION AND PULSATONAL PROPERTIES OF WOLF–RAYET STARS

Yu.A. Fadeyev¹

Institute of Astronomy of the Russian Academy of Sciences, Moscow

Submitted 12 May 2008

Evolution of Population I stars with initial masses ranging within $70M_{\odot} \leq M_{\text{ZAMS}} \leq 130M_{\odot}$ is considered under various assumptions on the mass loss rate \dot{M} . The mass–luminosity relation of W–R stars is shown to be most sensitive to the mass loss rate $\dot{M}_{3\alpha}$ during the helium burning phase. Together with the mass–luminosity relation obtained for all evolutionary sequences several more exact relations are determined for the constant ratios $0.5 \leq f_{3\alpha} \leq 3$, where $f_{3\alpha} = \dot{M}/\dot{M}_{3\alpha}$. Evolutionary models of W–R stars were used as initial conditions in hydrodynamic computations of radial nonlinear stellar oscillations. The oscillation amplitude is larger in W–R stars with smaller initial mass M_{ZAMS} or with lower mass loss rate \dot{M} due to higher surface abundances of carbon and oxygen. In the evolving W–R star the oscillation amplitude decreases with decreasing stellar mass M and for $M < 10M_{\odot}$ the sufficiently small nonlinear effects allow us to calculate the integral of the mechanical work W done over the pulsation cycle in each mass zone of the hydrodynamical model. The only positive maximum on the radial dependence of W is in the layers with temperature of $T \sim 2 \times 10^5$ K where oscillations are excited by the iron Z–bump κ –mechanism. Radial oscillations of W–R stars with mass of $M > 10M_{\odot}$ are shown to be also excited by the κ –mechanism but the instability driving zone is at the bottom of the envelope and pulsation motions exist in the form of nonlinear running waves propagating outward from the inner layers of the envelope.

Key words: stars – variable and peculiar

PACS numbers: 97.10.Cv; 97.10.Me; 97.10.Sj; 97.30.Eh

Introduction

During the core helium burning the structure of Population I stars with initial mass of $M_{\text{ZAMS}} \geq 30M_{\odot}$ weakly depends on the radial distribution of the mean molecular weight μ . This is due to the fact that radiation dominates in the internal energy, so that the hydrostatic equilibrium is governed by the gravity and by the gradient of radiation pressure whereas the gas pressure is negligible. Moreover, the opacity is mostly due to the Thompson scattering and radiative equilibrium above the convective core is almost independent of the radial distribution of μ .

¹e–mail: fadeyev@inasan.ru

Both these effects are strongest in stars with high effective temperature ($T_{\text{eff}} > 5 \times 10^4 \text{ K}$) and lead to the mass–luminosity relation of W–R stars (Langer, 1989; M. Beech, R. Mitalas, 1992).

Together with the mass–luminosity relation (Maeder, 1983; Doom et al., 1986; Maeder, 1987, Maeder, Meynet, 1987) W–R stars obey the mass–radius relation (Langer, 1989; Schaerer, Maeder, 1992) and therefore the sound travel time between the stellar center and the stellar surface can be considered approximately as a function of the stellar mass M . In recent years W–R stars were found to be unstable against radial oscillations (Glatzel et al., 1999; Fadeyev, Novikova, 2003; 2004; Dorfi et al., 2006; Fadeyev, 2007; Fokin, Tutukov, 2007; Fadeyev, 2008), so that one might assume that evolution of W–R stars is accompanied by decrease of the period of their radial oscillations Π . However one should bear in mind that if the pulsational instability is due to the iron Z–bump κ –mechanism (Dorfi et al., 2006; Fadeyev, 2008) then both the amplitude growth rate and the amplitude of radial oscillations depend on the chemical composition of the outer layers of the star. Such a dependence is still unclear and in the present paper we consider the pulsational properties of W–R stars with various surface abundances of helium, carbon and oxygen.

The chemical composition of outer layers of the evolving star depends on the both initial mass M_{ZAMS} and mass loss rate \dot{M} . In this paper we consider the Population I stars with initial masses ranging within $70M_{\odot} \leq M_{\text{ZAMS}} \leq 130M_{\odot}$. To evaluate the effect of uncertainties in empirical estimates of mass loss rates the evolutionary computations were carried out under various assumptions on \dot{M} . Some stellar models corresponding to the W–R phase were used as initial conditions in hydrodynamic computations of nonlinear radial stellar oscillations. In the present paper we continue our previous studies (Fadeyev, 2007; 2008) but now we use more recent data on the mass loss rate during helium burning that are most important for the structure of W–R stars.

Method of computations

Calculations of stellar evolution and stellar pulsations were done with methods that in general were described in the previous paper (Fadeyev, 2007), so that below only a few important changes are noted.

The mass loss rate during hydrogen burning and at the initial phase of helium burning \dot{M}_{H} was calculated according to Nieuwenhuijzen and de Jager (1990). The mass loss rate at the later stages of evolution $\dot{M}_{3\alpha}$ was calculated using the empirical formula by Nugis and Lamers (2000) which takes into account both clumping of the stellar wind and dependence of the mass loss rate on surface abundances of helium and heavier elements. In computations of stellar evolution the transition from \dot{M}_{H} to $\dot{M}_{3\alpha}$ was done during the initial stage of helium burning when the effective temperature of the contracting star reaches $T_{\text{eff}} = 10^4 \text{ K}$. At this

point of the evolutionary track the difference between \dot{M}_H and $\dot{M}_{3\alpha}$ is about a few percent. For example, for $M_{\text{ZAMS}} = 80M_\odot$ and $\dot{M} = \dot{M}_H$ the star reaches the effective temperature $T_{\text{eff}} = 10^4$ K when its mass is about $M = 37M_\odot$ and surface abundances of hydrogen and helium are $X(^1\text{H}) \approx 0.1$ and $X(^4\text{He}) \approx 0.88$, respectively. The mass loss rates evaluated with formulae by Nieuwenhuijzen and de Jager (1990) and by Nugis and Lamers (2000) are $\dot{M}_H = 9.3 \times 10^{-5}M_\odot/\text{yr}$ and $\dot{M}_{3\alpha} = 9.6 \times 10^{-5}M_\odot/\text{yr}$. It should be noted that during such a short phase of contraction of the star the evolutionary track crosses the H–R diagram so fast that variation of the threshold effective temperature by a factor of two around $T_{\text{eff}} = 10^4$ K does not affect perceptibly the later evolution of the stars.

Thus, in calculations of stellar evolution the mass loss rate was determined as

$$\dot{M} = \begin{cases} f_H \dot{M}_H, & \text{(hydrogen burning and initial helium burning),} \\ f_{3\alpha} \dot{M}_{3\alpha}, & \text{(helium burning at } T_{\text{eff}} \geq 10^4 \text{ K),} \end{cases} \quad (1)$$

where constant factors $1 < f_H < 2$ $0.5 < f_{3\alpha} < 3$ were introduced in order to evaluate the dependence of the results of evolution calculations on uncertainties in mass loss rates.

In previous papers (Fadeyev, 2007; 2008) the thermodynamic functions of the gas with temperature of $T < 10^7$ K were calculated using the OPAL equation of state data (Rogers et al., 1996). Unfortunately, these data are not quite appropriate at late stages of evolution when abundances of elements heavier than helium substantially increase in the outer layers of the star. In the present study we computed the tables of thermodynamic quantities for about three dozen compositions, so that both stellar evolution and pulsational instability can be selfconsistently calculated up to the core helium exhaustion when the stellar matter consists mostly of carbon and oxygen. Computing the tables of thermodynamic quantities we assumed that heavy elements are carbon, nitrogen, oxygen and neon. ZAMS abundances of these elements were taken from Rodgers et al. (1996).

The thermonuclear reaction network was extended to several dozen isotopes from hydrogen ^1H to nickel ^{56}Ni . However in comparison with previous computations the larger number of reactions did not affect significantly the results of evolution calculations. This is due to the fact that evolutionary calculations were terminated just after the helium exhaustion when the energy generation is due mostly to reactions of the tripple–alpha process and $\alpha(^{12}\text{C}, \gamma)^{16}\text{O}$.

Mass–luminosity relation

Domination of radiation in the helium burning phase leads to convergence of the evolutionary tracks of massive stars on the H–R diagram. In the upper panel of Fig. 1 are shown the parts of two evolutionary tracks with initial masses $M_{\text{ZAMS}} = 80M_\odot$ and $M_{\text{ZAMS}} = 130M_\odot$, both of them being computed with $f_H = f_{3\alpha} = 1$. At luminosity $\log L/L_\odot = 5.9$ masses and effective

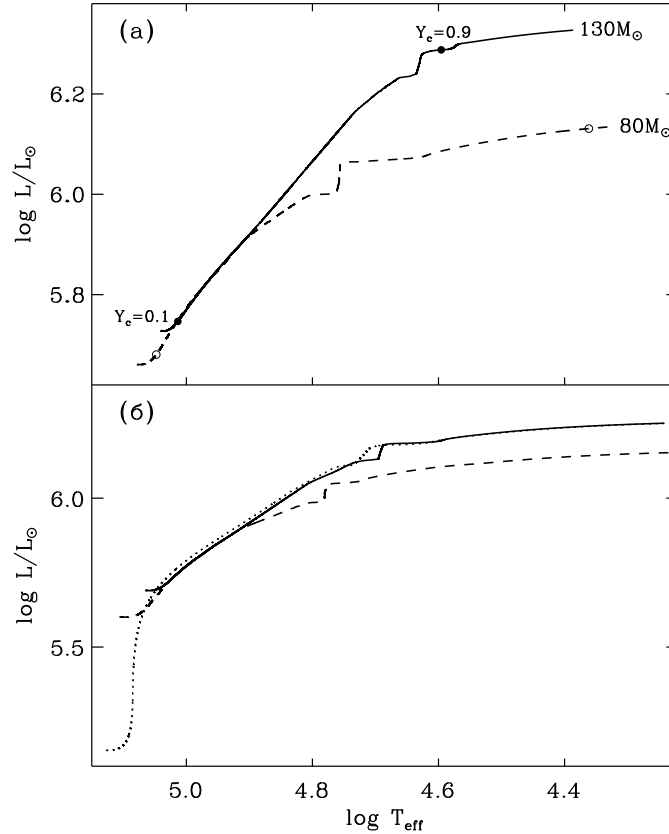


Figure 1: Upper panel: the parts of evolutionary tracks on the H–R diagram for initial masses $M_{\text{ZAMS}} = 130M_{\odot}$ (solid line) and $M_{\text{ZAMS}} = 80M_{\odot}$ (dashed line) with $f_{\text{H}} = f_{3\alpha} = 1$. The circles indicate the models with central helium abundance $Y_c = 0.9$ and $Y_c = 0.1$. Lower panel: The parts of evolutionary tracks of the star $M_{\text{ZAMS}} = 100M_{\odot}$ with $f_{\text{H}} = f_{3\alpha} = 1$ (solid line), $f_{\text{H}} = 2, f_{3\alpha} = 1$ (dashed line) and $f_{\text{H}} = 1, f_{3\alpha} = 2$ (dotted line).

temperatures of these stars ($M \approx 25M_{\odot}$, $T_{\text{eff}} \approx 8.2 \times 10^4$ K) differ from one another by 2% and 0.1%, respectively.

W–R stars with close values of the stellar mass M , luminosity L and radius R but with different initial masses M_{ZAMS} have significantly different radial distributions of the mean molecular weight. This is illustrated in the upper panel of Fig. 2 where for two models of W–R stars with mass of $M = 25M_{\odot}$ ($M_{\text{ZAMS}} = 80M_{\odot}$ and $M_{\text{ZAMS}} = 130M_{\odot}$) the radial dependencies of the helium abundance $X(^4\text{He})$ are plotted as a functions of the Lagrangean mass coordinate M_r . The lower helium abundance and the higher carbon abundance in outer layers of the star with larger initial mass M_{ZAMS} is due to the more efficient helium burning during the preceding stellar evolution. Homogeneity of the chemical composition within the large mass fraction of the star is due to the large extension of convective cores.

Dependence of the evolution of W–R stars on the mass loss rate is illustrated in the lower panel of Fig. 1 where three evolutionary tracks of the star with initial mass of $M_{\text{ZAMS}} = 100M_{\odot}$ are plotted for three different cases of the mass loss: ($f_{\text{H}} = f_{3\alpha} = 1$), ($f_{\text{H}} = 2, f_{3\alpha} = 1$) and

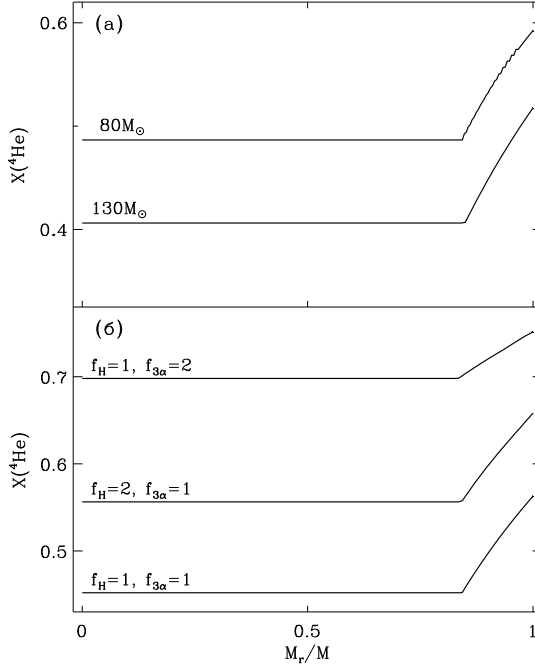


Figure 2: Relative mass abundance of helium $X(^4\text{He})$ as a function of the Lagrangean mass coordinate M_r in W–R stars with mass of $M = 25M_\odot$. Upper panel: the case of mass loss $f_{\text{H}} = f_{3\alpha} = 1$. Numbers at the curves indicate the initial stellar mass M_{ZAMS} . Lower panel: three different cases of mass loss for $M_{\text{ZAMS}} = 100M_\odot$.

($f_{\text{H}} = 1, f_{3\alpha} = 2$). Doubling the mass loss rate \dot{M}_{H} during hydrogen burning leads to decrease of the luminosity of the W–R star with mass of $M = 25M_\odot$ by about $\approx 3\%$, whereas the core helium abundance increases by $\Delta Y_c \approx 0.1$.

The most important role in the structure of W–R stars belongs to the mass loss rate during the helium burning. For example, doubling $\dot{M}_{3\alpha}$ leads to decrease of the luminosity in the W–R star with mass of $M = 25M_\odot$ by $\approx 9\%$ and at the same time to increase of the core helium abundance by $\Delta Y_c \approx 0.25$. Dependence of the radial distribution of helium abundance $X(^4\text{He})$ on the mass loss rate $\dot{M}_{3\alpha}$ is shown in the lower panel of Fig. 2. Moreover, increase of $\dot{M}_{3\alpha}$ is accompanied by the slower growth of the central temperature, so that the end of core helium exhaustion occurs at the lower stellar mass and on the H–R diagram the evolutionary track extends to lower luminosities.

Convergence of the evolutionary tracks on the H–R diagram implies the existence of the correlation between the stellar mass M and the stellar luminosity L . Fig. 3 shows the mass–luminosity diagram with two pairs of evolutionary tracks for two initial stellar masses ($M_{\text{ZAMS}} = 90M_\odot, M_{\text{ZAMS}} = 130M_\odot$) and two cases of mass loss: ($f_{\text{H}} = 1, f_{3\alpha} = 1; f_{\text{H}} = 2, f_{3\alpha} = 1$). At the final point of each track plotted in Fig. 3 the central helium abundance is $Y_c \approx 10^{-3}$. It is clearly seen that during the significant part of the helium burning phase the stellar mass and luminosity are nearly related by the power dependence. The position of the initial point of the

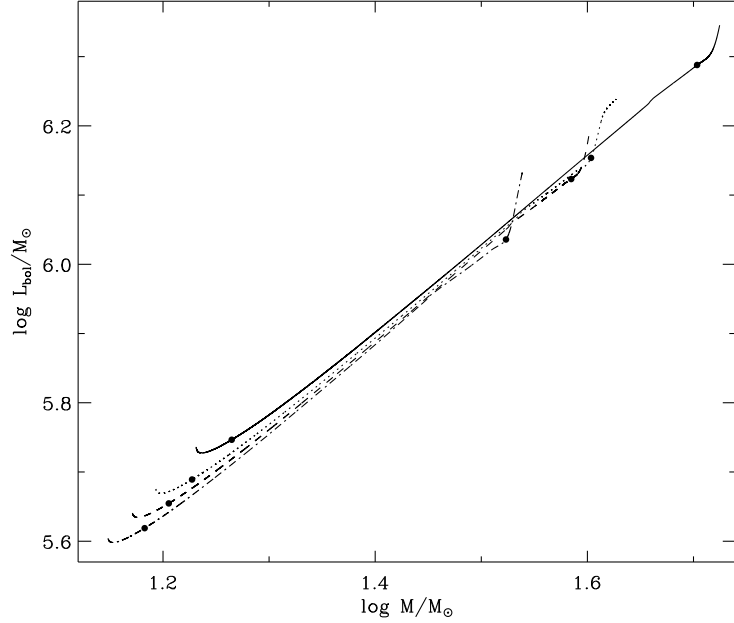


Figure 3: Mass–luminosity relation for $f_H = 1$ and $f_H = 2$ at initial masses $M_{\text{ZAMS}} = 130M_\odot$ (solid and dashed lines) and $M_{\text{ZAMS}} = 90M_\odot$ (dotted and dashed–dotted lines). For all models $f_{3\alpha} = 1$.

power dependence changes with initial stellar mass and mass loss rate. For example, the central helium abundance at the initial point ranges from $Y_c = 0.85$ for $M_{\text{ZAMS}} = 70M_\odot$ to $Y_c = 0.94$ for $M_{\text{ZAMS}} = 130M_\odot$. For smaller M_{ZAMS} or larger \dot{M}_H the helium burning occurs at the lower central temperature, so that on the mass–luminosity diagram the part of the track with power dependence moves to smaller values of M and L .

The parts of evolutionary tracks that can be approximated by the power dependence on the mass–luminosity diagram are displayed in Fig. 4. The maximum deviation of each track from the power dependence is $\Delta_L = \max |\Delta \log L| \approx 0.01$ for $0.5 \leq f_{3\alpha} \leq 2$ and $\Delta_L \approx 0.03$ for $f_{3\alpha} = 3$. The linear fit on the $(\log M, \log L)$ plane for models with $70M_\odot \leq M_{\text{ZAMS}} \leq 130M_\odot$, $1 \leq f_H \leq 2$ and $0.5 \leq f_{3\alpha} \leq 3$ shown in Fig. 4 is given by

$$\log L/L_\odot = 3.675 + 1.568 \log M/M_\odot. \quad (2)$$

The maximum deviation of the parts of evolutionary tracks from relation (2) is $\Delta_L \leq 0.11$ and its large value is due to the dependence of the coefficients of this relation on the mass loss rate $\dot{M}_{3\alpha}$. Therefore, more exact approximation can be obtained for fixed values of $f_{3\alpha}$:

$$\log L/L_\odot = \begin{cases} 4.236 + 1.212 \log M/M_\odot, & (f_{3\alpha} = 0.5, \quad \Delta_L \leq 0.06), \\ 4.099 + 1.282 \log M/M_\odot, & (f_{3\alpha} = 1, \quad \Delta_L \leq 0.03), \\ 3.821 + 1.454 \log M/M_\odot, & (f_{3\alpha} = 2, \quad \Delta_L \leq 0.02), \\ 3.632 + 1.580 \log M/M_\odot, & (f_{3\alpha} = 3, \quad \Delta_L \leq 0.04). \end{cases} \quad (3)$$

It should be noted that the mass interval within which formulae (3) can be applied depends on the initial mass M_{ZAMS} as well as on parameters f_H and $f_{3\alpha}$. The stellar mass M and the

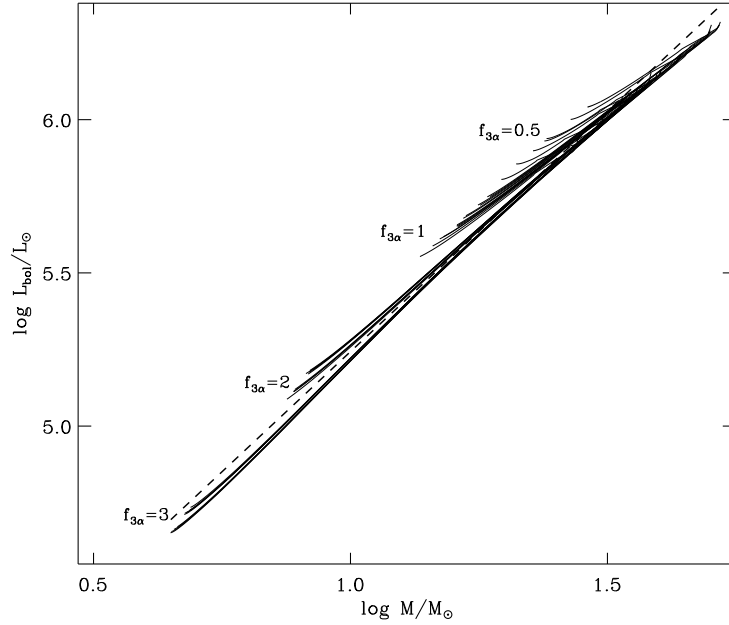


Figure 4: Mass–luminosity relation of W–R stars with $70M_{\odot} \leq M_{\text{ZAMS}} \leq 130M_{\odot}$, $1 \leq f_{\text{H}} \leq 2$ and $0.5 \leq f_{3\alpha} \leq 3$. The dashed line shows relation (refwrm11).

central helium abundance Y_c corresponding to limits of these intervals are given in Table 1. The last column of Table 1 gives the evolution time t_{ev} for this interval.

When one considers the stellar mass M as a parameter one should bear in mind that the stellar evolution becomes slower as M decreases. In Fig. 5 for $M_{\text{ZAMS}} = 100M_{\odot}$ and $f_{\text{H}} = 1$ are shown the plots of the life time Δt_{ev} within the mass interval $[M - \Delta M, M]$, where $\Delta M = 0.5M_{\odot}$. The plots shown in Fig. 5 weakly depend on M_{ZAMS} and f_{H} . The growth of the life time Δt_{ev} with increasing $f_{3\alpha}$ is due to the slower increase of the central temperature and slower conversion of helium into carbon. For initial stellar mass $M_{\text{ZAMS}} = 100M_{\odot}$ and mass loss rate during hydrogen burning $f_{\text{H}} = 1$ the second half of the life time correspond to W–R masses $M < 33M_{\odot}$, $M < 25M_{\odot}$, $M < 12M_{\odot}$ and $M < 7M_{\odot}$ for $f_{3\alpha} = 0.5, 1, 2$ and 3 , respectively.

Nonlinear radial oscillations

During evolution of the W–R star the relative radius of the stellar core increases, so that both the sound travel time from the center to the surface and the period of radial oscillations gradually decrease. At the same time the instability excitation zone moves closer to the stellar surface and the amplitude of oscillations decreases due to diminishing mass of the driving zone. Decrease of the amplitude and the period of radial oscillations in evolving W–R stars is shown in Fig. 6 where for stars with initial masses $M_{\text{ZAMS}} = 90M_{\odot}$ and $M_{\text{ZAMS}} = 120M_{\odot}$ are given the plots of the maximum expansion velocity of the outer boundary of the hydrodynamic model U_{max} expressed in units of the local escape velocity v_{esc} and the period of radial oscillations Π .

Table 1: Limiting values of stellar mass M and central helium abundance Y_c in the mass–luminosity relations (3).

$f_{3\alpha}$	f_H	M_{ZAMS}/M_\odot	M/M_\odot		Y_c		$t_{\text{ev}}, 10^6 \text{ yr}$
0.5	1	80	36.2	24.1	0.85	0.02	0.29
		120	50.1	28.9	0.93	0.05	0.27
	2	80	31.1	21.0	0.86	0.02	0.31
		120	38.4	23.8	0.92	0.03	0.30
1.0	1	80	36.1	16.6	0.88	0.09	0.28
		120	50.1	18.7	0.95	0.14	0.26
	2	80	31.0	14.4	0.90	0.08	0.30
		120	38.2	16.1	0.94	0.12	0.28
2.0	1	80	35.6	8.5	0.88	0.08	0.36
		120	49.9	8.2	0.95	0.05	0.41
	2	80	31.0	7.7	0.92	0.08	0.38
		120	38.3	7.8	0.95	0.07	0.40
3.0	1	80	36.2	4.9	0.90	0.01	0.54
		120	50.4	4.7	0.96	0.01	0.58
	2	80	31.2	4.5	0.94	0.01	0.59
		120	38.5	4.6	0.96	0.02	0.58

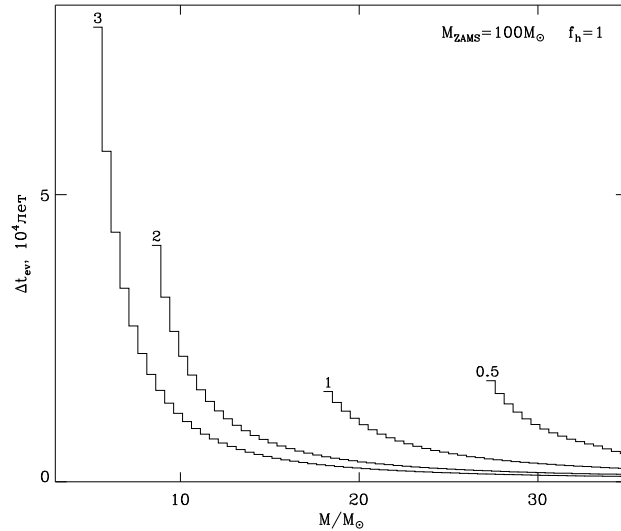


Figure 5: The life time Δt_{ev} of W–R stars within the mass interval $\Delta M = 0.5 M_\odot$ as a function of the stellar mass M . The initial mass is $M_{\text{ZAMS}} = 100 M_\odot$ and $f_H = 1$. The numbers at the curves indicate correspondig values of $f_{3\alpha}$.

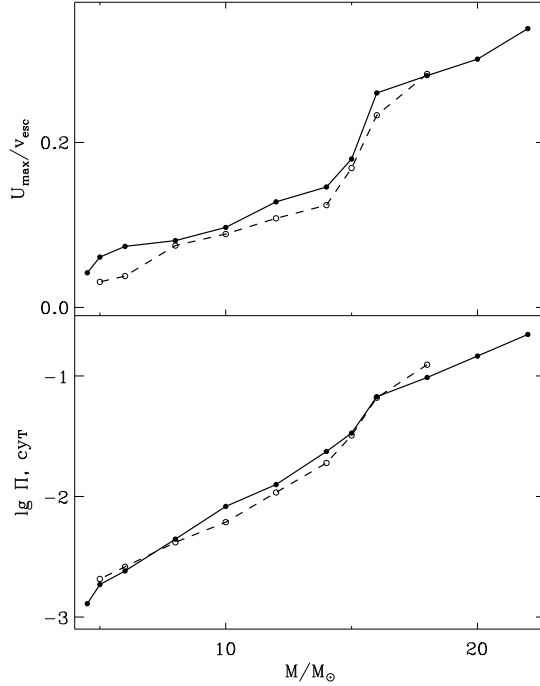


Figure 6: The ratio of the maximum expansion velocity of the outer boundary U_{\max} to the local escape velocity v_{esc} (upper panel) and the period of radial oscillations Π in days (lower panel) as a function of the stellar mass M . In solid and dashed lines are shown the evolutionary sequences with $M_{\text{ZAMS}} = 120M_{\odot}$ and $M_{\text{ZAMS}} = 90M_{\odot}$, respectively.

The growth time of radial oscillations is of the order of the stellar dynamic time scale, so that oscillations of W–R stars are strongly nonadiabatic. In contrast to many other radially pulsating stars oscillations of W–R stars cannot be described in terms of the standing wave since the kinetic energy of the pulsating envelope only once per period passes the minimum and the maximum. Radial oscillations of W–R stars should be considered as nonlinear running waves propagating from the envelope bottom to the outer boundary. That is why in W–R stars with mass of $M > 15M_{\odot}$ the pulsation constant ($Q \geq 0.1$ day) is significantly larger in comparison with pulsation constants of stars radially pulsating in the form of standing waves. The only exception is W–R stars with mass of $M < 10M_{\odot}$ where the small-amplitude radial oscillations can be approximately represented by nonadiabatic standing waves.

In the stellar mass range of $4.5M_{\odot} \leq M \leq 20M_{\odot}$ the pulsation constant of W–R stars can be approximately written as

$$\log Q = -2.6 + 0.1M_{\odot}. \quad (4)$$

Properties of some hydrodynamic models are listed in Table 2. The mass of outer pulsating layers is negligible in comparison with the total mass of the star, so that the abundances of helium $X(^4\text{He})$, carbon $X(^{12}\text{C})$ and oxygen $X(^{16}\text{O})$ are constant through the envelope. The mean pulsation period Π was evaluated using the discrete Fourier transform of the kinetic energy of the oscillating envelope within the time interval $10^2 \lesssim t/\Pi \lesssim 10^3$. However, strictly

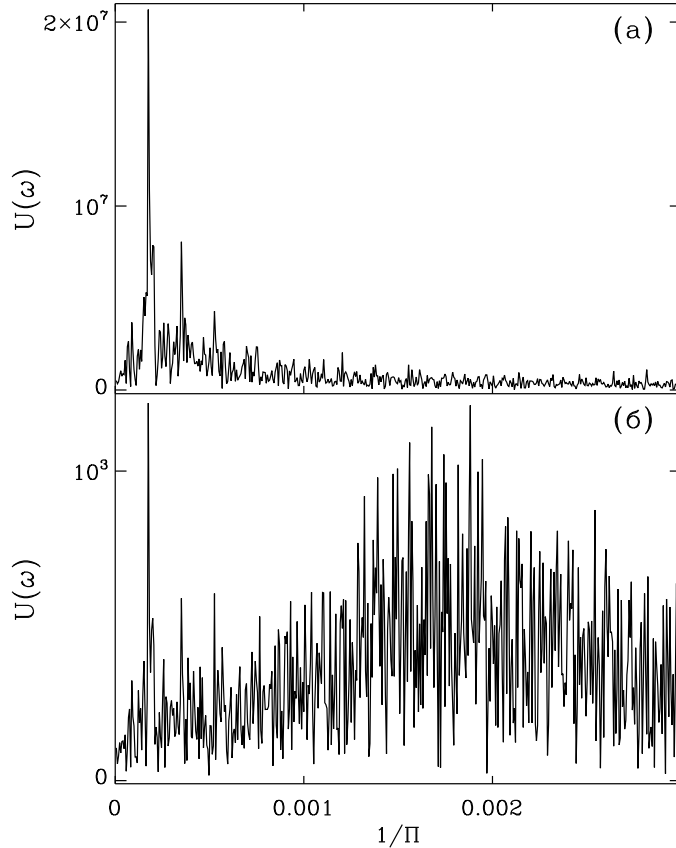


Figure 7: The power spectrum of velocity $U(\omega)$ in the outer (upper panel) and the inner (lower panel) layers of the W–R star with mass $M = 16M_{\odot}$.

speaking, the definition of the period of radial oscillations can be applied to W–R stars with rather low stellar masses because for $M > 15M_{\odot}$ the frequency of oscillations at the bottom of the envelope becomes somewhat higher than that of the outer layers. In Fig. 7 are shown the power spectra of the velocity of gas in the outer ($r \approx R$) and the inner ($r \approx 0.79R$) layers of the envelope of the W–R star with mass of $M = 16M_{\odot}$. Contribution of short–period oscillations in the inner layers becomes significant in stars with $M > 20M_{\odot}$ because they affect the radiative flux emerging from the outer boundary and the period of light variations becomes shorter than that of hydrodynamic motions in the outer layers of the pulsating envelope.

As is seen in Table 2 the pulsational properties of W–R stars depend mostly on the mass loss rate $\dot{M}_{3\alpha}$ whereas the role of the both initial stellar mass M_{ZAMS} and mass loss rate during hydrogen burning \dot{M}_{H} is significantly weaker. This is due to the fact that variations of $\dot{M}_{3\alpha}$ are accompanied by significant changes of the both stellar luminosity and surface abundances of carbon and oxygen. In particular, increase of the mass loss rate during helium burning leads to the smaller stellar luminosity and therefore to the smaller nonadiabaticity of stellar pulsations.

An important consequence of nonlinear radial stellar oscillations is the increase of the mean radius of pulsating layers of the gas. This effect is illustrated by Table 2 where the last column gives the mean radius of the outer boundary of the hydrodynamic model \bar{R} expressed in units

Table 2: Properties of some hydrodynamic models of W–R stars.

$M_{\text{ZAMS}}/M_{\odot}$	$f_{3\alpha}$	M/M_{\odot}	$\log L/L_{\odot}$	$X(^4\text{He})$	$X(^{12}\text{C})$	$X(^{16}\text{O})$	Π day	$U_{\text{max}}/v_{\text{esc}}$	\bar{R}/R	
90	2	15	5.541	0.639	0.311	0.031	0.0525	0.21	2.1	
		10	5.272	0.467	0.436	0.078	0.0085	0.13	1.1	
	3	18	5.660	0.786	0.186	0.009	0.124	0.30	3.4	
		15	5.524	0.745	0.223	0.014	0.0321	0.17	1.5	
		10	5.221	0.635	0.316	0.030	0.0061	0.09	1.1	
		5	4.733	0.368	0.502	0.111	0.0021	0.03	1.0	
120	2	15	5.553	0.634	0.315	0.033	0.0652	0.25	2.5	
		10	5.289	0.461	0.439	0.081	0.0107	0.14	1.2	
	3	22	5.772	0.827	0.148	0.006	0.221	0.34	6.4	
		20	5.712	0.807	0.166	0.008	0.146	0.30	3.8	
		15	5.528	0.742	0.225	0.014	0.0336	0.18	1.5	
		10	5.248	0.632	0.319	0.031	0.0083	0.11	1.1	
			5	4.743	0.369	0.501	0.111	0.0018	0.06	1.0

of the initial equilibrium radius R .

Mechanism of pulsational instability

The elementary spherical layer of gas contributing into excitation of pulsational instability performs the positive mechanical work during the pulsation cycle, that is the integral of mechanical work is positive : $W = \oint PdV > 0$, where P is the total pressure and V is the specific volume. Unfortunately, for hydrodynamical models of W–R stars exact calculation of the radial dependence of the mechanic work W is impossible because of strongly nonlinear radial oscillations. The only exception is W–R stars with mass of $M \leq 10M_{\odot}$ where pulsation motions are characterized by a good repetition of pulsation cycles. Formation of W–R stars with so small masses implies rather high mass loss rates during the core helium burning phase ($f_{3\alpha} \geq 3$). Omitting discussion on possibility of the existence of such W–R stars we consider their pulsational properties because the results obtained can be generalized to more massive W–R stars undergoing substantially smaller mass loss.

The upper panel of Fig. 8 shows radial dependences of the inetgral of mecahnical work W for two models of W–R stars with mass of $M = 6M_{\odot}$ and $M = 8M_{\odot}$. It is clearly seen that excitation of oscillations ($W > 0$) occurs in the outer layers of the stars and the maximum of W moves to the surface as the stellar mass M decreases. To clarify the origin of the pulsational instability one should compare the radial dependence of W with that of the amplitude of

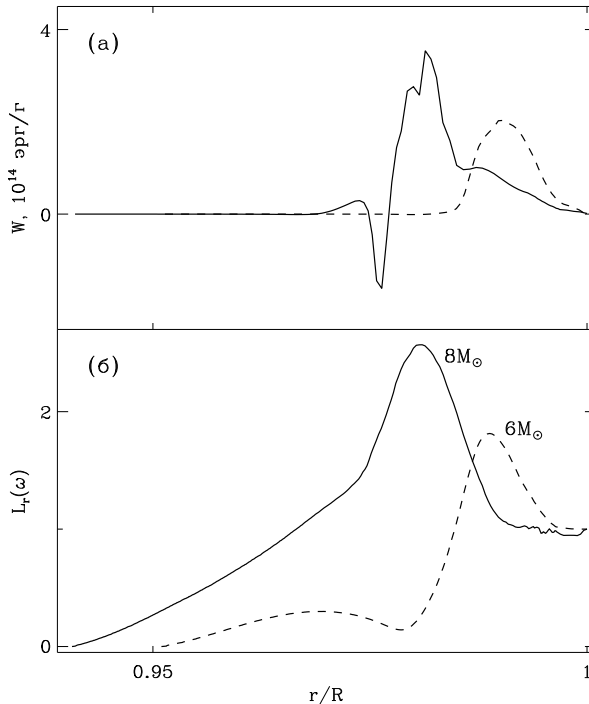


Figure 8: Radial dependences of the mechanical work over the pulsation cycle W (upper panel) and the normalized spectral density of luminosity $L_r(\omega)$ (lower panel) for models of W–R stars with masses $M = 6M_\odot$ and $M = 8M_\odot$.

radiative flux variations. To this end we consider the spectral density of luminosity

$$L_r(\omega) = \int_{-\infty}^{\infty} L_r e^{i\omega t} dt \quad (5)$$

at the angular frequency $\omega = 2\pi/\Pi$. The spectral density $L_r(\omega)$ was computed in all Lagrangean mass zones using the discrete Fourier transform within time intervals $t/\Pi \lesssim 10^3$. The lower panel of Fig. 8 shows two radial dependences of $L_r(\omega)$ that are normalized to the surface value.

Coincidence of radial coordinates of maxima of W and $L_r(\omega)$ (see Fig. 8) allows us to conclude that excitation of oscillations is due to the interaction of radiative flux with gas of the envelope. In particular, for $W > 0$ it is necessary that the gas absorbs radiation at maximum compression and becomes more transparent at maximum expansion. Fig. 9 shows the plots of variations of the gas density ρ and opacity κ in the mass zone with maximum mechanical work W of the model of W–R stars with mass $M = 8M_\odot$. It is clearly seen that the positive mechanical work W is due to the κ -mechanism. The average temperature of gas in this zone is $T \sim 2 \times 10^5$ K and the positive temperature derivative of opacity $(\partial \ln \kappa / \partial \ln T)_\rho > 0$ is due to the iron Z-bump.

Fig. 10 shows the plots of radial dependencies of the gas density ρ and the spectral density of luminosity $L_r(\omega)$ for outer layers of W–R stars with masses $12M_\odot \leq M \leq 18M_\odot$. The

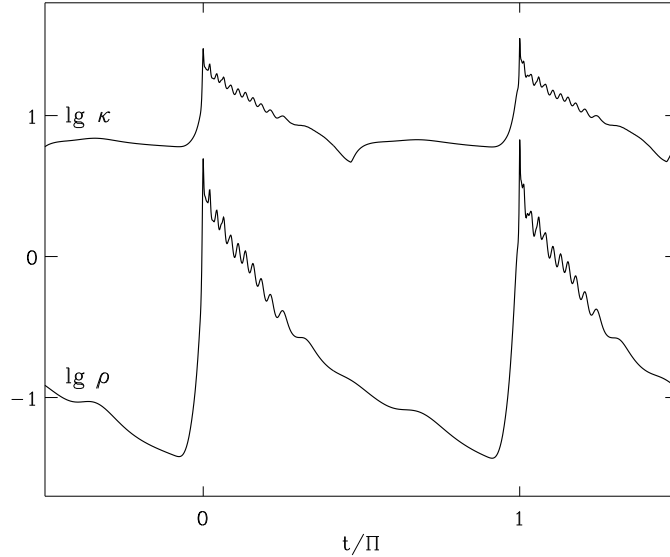


Figure 9: Variations of the gas density ρ and opacity κ in the vicinity of the maximum of mechanical work W in the model of the W–R star with mass $M = 8M_{\odot}$. The plots of ρ and κ are arbitrarily shifted along the vertical axis.

narrow maximum of $L_r(\omega)$ (see the lower panel of Fig. 10) corresponds to layers with average temperature $T \sim 2 \times 10^5$ K where the gas density ρ and opacity κ reach the maximum simultaneously, that is excitation of oscillations is also due to the κ –mechanism. In layers above the excitation zone $\partial L_r(\omega)/\partial r \approx 0$, that is there are neither excitation nor damping zones. More massive W–R stars possess more extended envelopes with smaller gradient of the gas density. The excitation zone is at the bottom of the envelope and radial oscillations exist as successive nonlinear waves propagating from the outer boundary of the core to the stellar surface.

Conclusion

As follows from results presented above the mass and luminosity of Population I massive stars are related by the power dependence during the large part of the helium burning phase. Boundaries of the segment of the evolutionary track within which the coefficients of the power dependence are constant depends on the initial stellar mass M_{ZAMS} and the mass loss rate \dot{M} during the preceding evolution. At the initial point of the power dependence the central helium abundance ranges from $Y_c \approx 0.78$ ($M_{\text{ZAMS}} = 70M_{\odot}$, $f_{3\alpha} = 0.5$) to $Y_c \approx 0.96$ ($M_{\text{ZAMS}} = 130M_{\odot}$, $f_{3\alpha} = 3$), whereas the effective temperature is in the range from $T_{\text{eff}} \approx 3 \times 10^4$ K ($M_{\text{ZAMS}} = 120M_{\odot}$) to $T_{\text{eff}} \approx 5 \times 10^4$ K ($M_{\text{ZAMS}} = 70M_{\odot}$). At the end of the power dependence the central helium abundance ranges within $0.01 \lesssim Y_c \lesssim 0.15$. Thus, the limits of applicability of the mass–luminosity relation depend on the both initial mass M_{ZAMS} and mass loss rate \dot{M} , so that relations (3) should be used with corresponding boundary values of the stellar mass M listed in Table 1.

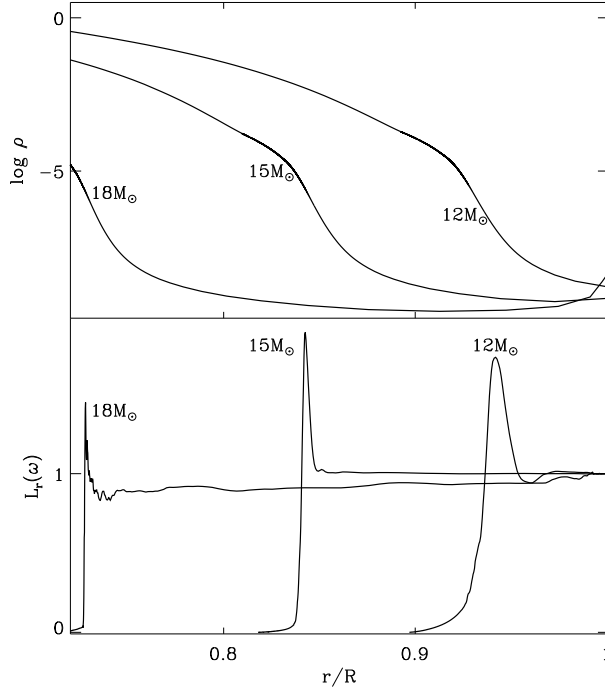


Figure 10: Radial dependencies of gas density ρ (upper panel) and normalized spectral density of luminosity $L_r(\omega)$ (lower panel) in W–R stars with mass $M = 12M_{\odot}$, $15M_{\odot}$ and $18M_{\odot}$.

In the present study we considered pulsational properties of W–R stars as a function of three parameters: the initial stellar mass M_{ZAMS} , the mass loss rate during hydrogen burning \dot{M}_{H} and the mass loss rate during the helium burning phase $\dot{M}_{3\alpha}$. However the most important is $\dot{M}_{3\alpha}$ since its variations lead to significant changes in surface abundances of helium, carbon and oxygen. In particular, at lower mass loss rate $\dot{M}_{3\alpha}$ radial oscillations of W–R stars have larger amplitudes due to higher surface abundances of carbon and oxygen.

As is seen from Fig. 6 and Table 2 the period of radial oscillations is a sensitive indicator of the stellar mass and during evolution of the W–R star decreases from ≈ 5.5 hr at $M = 22M_{\odot}$ to ≈ 2.6 min at $M = 5M_{\odot}$. Thus, observational estimates of pulsation periods could provide with a direct evaluation of the masses of W–R stars. For example, according to Veen et al. (2002a, 2002b, 2002c) the pulsation period of WR46 is $\Pi \approx 0.14$ day and as follows from our hydrodynamical calculations the stellar mass is $M \approx 20M_{\odot}$.

The present study is confined to hydrodynamical models of W–R stars near their final stage of evolution and such a choice is to their longer life time. However of great interest are more massive W–R stars with higher luminosity and much stronger instability similar to that of LBV stars. The study of these objects will be presented in the forthcoming paper.

References

1. M. Beech, R. Mitalas, *Astron. Astrophys.*, **262**, 483 (1992).
2. P.M. Veen, A.M. van Genderen, K.A. van der Hucht, et al., *Astron.Astrophys.*, **385**, 585 (2002).
3. P.M. Veen, A.M. van Genderen, K.A. van der Hucht, et al., *Astron.Astrophys.*, **385**, 600 (2002).
4. P.M. Veen, A.M. van Genderen, K.A. van der Hucht, et al., *Astron.Astrophys.*, **619**, 585 (2002).
5. E.A. Dorfi, A. Gautschy, H. Saio, *Astron.Astrophys.*, **453**, L35 (2006).
6. C. Doom, J.P. de Greve, C. de Loore, *Astrophys. J.*, **303**, 136 (1986).
7. W. Glatzel, M. Kiriakidis, S. Chernigovskij, et al., *MNRAS*, **303**, 116 (1999).
8. N. Langer, *Astron. Astrophys.*, **210**, 93 (1989).
9. A. Maeder, *Astron. Astrophys.*, **120**, 113 (1983).
10. A. Maeder, *Astron. Astrophys.*, **173**, 247 (1987).
11. A. Maeder, G. Meynet, *Astron. Astrophys.*, **182**, 243 (1987).
12. N. Nugis, H. J. G. L. M. Lamers, *Astron. Astrophys.*, **360**, 227 (2000).
13. H. Nieuwenhuijzen and C. de Jager, *Astron.Astrophys.*, **231**, 134 (1990).
14. F.J. Rogers, F.J. Swenson, and C.A. Iglesias, *Astrophys.J.*, **456**, 902 (1996).
15. Yu.A. Fadeyev, M.F. Novikova, *Ast.Let.*, **29**, 522 (2003).
16. Yu.A. Fadeyev, M.F. Novikova, *Ast.Let.*, **30**, 707 (2004).
17. Yu.A. Fadeyev, *Ast.Let.*, **33**, 692 (2007).
18. Yu.A. Fadeyev, *Ast.Rep.*, in press (2008).
19. A.B. Fokin, A.V. Tutukov, *Ast.Rep*, **51**, 742 (2007).
20. D. Schaerer, A. Maeder, *Astron. Astrophys.*, **263**, 192 (1992).